Extraordinary Improvement of the Graphitic Structure of Continuous Carbon Nanofibers Templated with Double Wall Carbon Nanotubes

Dimitry Papkov,[†] Allison M. Beese,[‡] Alexander Goponenko,[†] Yan Zou,[†] Mohammad Naraghi,[‡] Horacio D. Espinosa,[‡] Biswajit Saha,[§] George C. Schatz,[§] Alexander Moravsky,[⊥] Raouf Loutfy,[⊥] Sonbinh T. Nguyen,[§] and Yuris Dzenis[†,*]

[†]Department of Mechanical and Materials Engineering, Nebraska Center for Materials and Nanoscience, University of Nebraska-Lincoln, Lincoln, Nebraska 68588-0526, United States, [‡]Department of Mechanical Engineering and [§]Department of Chemistry, Northwestern University, Evanston, Illinois 60208, United States, and [⊥]MER Corporation, 7960 South Kolb Road, Tucson, Arizona 85706, United States

ABSTRACT Carbon nanotubes are being widely studied as a reinforcing element in high-performance composites and fibers at high volume fractions. However, problems with nanotube processing, alignment, and non-optimal stress transfer between the nanotubes and surrounding matrix have so far prevented full utilization of their superb mechanical properties in composites. Here, we present an alternative use of carbon nanotubes, at a very small concentration, as a templating agent for the formation of graphitic structure in fibers. Continuous carbon nanofibers (CNF) were manufactured by electrospinning from polyacrylonitrile (PAN) with 1.2% of double wall nanotubes (DWNT). Nanofibers were oxidized and carbonized at temperatures from 600 °C to 1850 °C. Structural analyses revealed significant improvements in graphitic structure and crystal orientation in the templated CNFs, with the largest improvements observed at lower carbonization temperatures. *In situ* pull-out experiments showed good interfacial bonding between the DWNT bundles and the surrounding templated carbon matrix. Molecular Dynamics (MD) simulations of templated carbonization confirmed oriented graphitic growth and provided insight into mechanisms of carbonization initiation. The obtained results indicate that global templating of the graphitic structure in fine CNFs can be achieved at very small concentrations of well-dispersed DWNTs. The outcomes reveal a simple and inexpensive route to manufacture continuous CNFs with improved structure and properties for a variety of mechanical and functional applications. The demonstrated improvement of graphitic order at low carbonization temperatures in the absence of stretch shows potential as a promising new manufacturing technology for next generation carbon fibers.

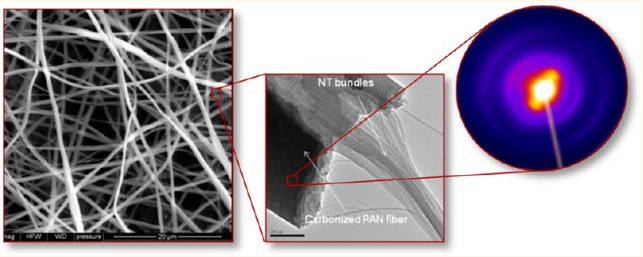

KEYWORDS: continuous carbon nanofibers · double-wall carbon nanotubes · carbonization templating · graphitic structure · molecular dynamics simulations

Recent discoveries of new nanocarbon allotropes[1] and subsequent demonstrations of superior mechanical properties for two of these allotropes, carbon nanotubes (NT), and graphene, have raised hopes for new structural materials with extraordinary mechanical performance. However, after two decades of intensive research, a viable carbon nanotube-reinforced supernanocomposite, defined as a bulk composite with properties exceeding the properties of existing advanced composites,[2,3] is yet to be demonstrated. The problems are well-documented and include difficulties with NT dispersion, NT alignment, achieving a high volume fraction of NT, and optimizing stress transfer to NTs. It is still difficult to make a high-quality NT–polymer composite with a volume fraction of nanotubes higher than a few percent.[1] As a result, most current and projected near-term applications of nanotube composites appear to rely on the thermal and electrical properties of NTs rather than their mechanical superiority.[1,4]

The situation is only slightly better for NT-reinforced fibers. Fibers are ideally suited for nanoreinforcement because of their small

* Address correspondence to ydzenis@unl.edu.

Received for review July 30, 2012 and accepted November 24, 2012.

Published online December 18, 2012
10.1021/nn303423x

(micrometer) diameter. Polymer fibers are highly aligned and their processing methods can naturally lead to high NT alignment. Numerous researchers have manufactured and studied NT-reinforced polymer fibers (see, for example refs 5−10). However, solution-, gel- or melt-spun fibers still usually suffer from the general problems of the NT composites mentioned above. As a result, only slight improvements in mechanical properties were typically reported, while sometimes the reinforcing effects were negative.[6]

Perhaps recognizing the above processing problems, several new manufacturing techniques have been developed to produce neat or near-neat NT fibers and yarns. These include spinning from surfactant-stabilized NT solutions with subsequent coagulation in polymer solution flow,[11−13] superacid solution spinning,[14,15] direct solid-state spinning from NT aerogels formed in the chemical vapor deposition (CVD) reactor,[16−18] solid-state spinning from vertically grown NT arrays or forests,[19−25] and twist-stretching CVD-grown NT ribbons.[26] Often, the resulting fibers and yarns were further impregnated with polymers or otherwise densified and postprocessed. These high NT-fraction yarns and fibers are usually very lightweight (highly porous), even after densification. Such fibers demonstrated ultrahigh specific toughness and some also demonstrated high strength.[26] However, neat NT fiber strength and stiffness values achieved to date, even when calculated per NT content (*i.e.*, ignoring voids in the fiber cross-section), still remain significantly lower than the strength and modulus of commercial carbon fibers, and far below the property levels of NT themselves. The highest reported strength values in the references above[11−26] range from 8% to about 45% of the strength of the best commercial carbon fibers. Key reasons cited for the low values were poor stress transfer between the NT bundles in the yarns and nonoptimal hierarchical yarn architecture. It was shown, for example, that poor stress transfer was responsible for the total energy stored in NT being only a few percent of the maximum possible energy in the bundles.[26]

Neat graphene and graphene oxide (GO) fibers were also recently manufactured.[27,28] Mechanical properties of these early samples were relatively low. These properties will undoubtedly improve with more research; yet, high volume fraction graphene and GO fibers will likely face some of the same challenges faced by the NT fibers.

Better fundamental understanding of the complex multiscale mechanisms of deformation and failure in NT materials[26,29] will lead to qualitative improvements and new design and manufacturing methodologies. However, full utilization of superb intrinsic properties of nanocarbons in bulk structural materials may be further away now than it seemed a decade ago.[1]

An alternative way to use nanocarbons in structural materials may be to utilize them in small quantities as catalysts, nuclei, or "templates," for directed crystallization or other structural transformations. Such applications would utilize the ultrahigh specific surface area of NTs or graphene/graphene oxide and their potential strong interaction with surrounding materials. These templated materials could also be economically viable as the relatively expensive nanocarbons would be utilized in low quantities and their dispersion and processing would be significantly easier than in the case of high volume fraction materials. Strong nanocarbons could potentially deliver synergistic simultaneous structural improvements and reinforcement.

Carbon nanotubes have been shown to improve crystallization and chain orientation in polypropylene and polyacrylonitrile (PAN) fibers.[5,6,30] Graphene−polymer nanocomposites show dramatic reduction in the glass transition temperature and improved mechanical properties at low graphene content.[31,32] However, as pointed out in ref 1, from the standpoint of structural materials, adding graphene platelets to polymers is not a transformational application, it is an incremental improvement, however considerable. Ultralow volume fraction polymer nanocomposites cannot compete with advanced composites, such as carbon-epoxy.

An intriguing opportunity to achieve a more significant property change presents itself in carbon materials, particularly carbon fibers. Carbon fibers are the strongest commercial material today and they dominate the advanced composites market. After four decades of development, their property levels appear to have reached saturation. Modern efforts are mostly focused on improved quality control and cost reduction. However, the incorporation of NTs or graphene into carbon fibers might change the carbon structure and further improve properties. Nanocarbons are ideally suited as both reinforcement and possible structural change agent for carbon fibers. Incorporation of NTs in carbon microfibers has been shown to result in improved graphitic order and mechanical properties.[33−35] However, good nanotube orientation is difficult to achieve in fibers with micrometer-size diameters. The reported properties of the NT-modified fibers[33−35] are still lower than the properties of commercial fibers.

Carbon nanofibers (CNF) are finding increasing use in a broad variety of nanotechnology applications.[36,37] Continuous carbon nanofibers can be produced by carbonization of electrospun polymer precursors. Top-down electrospinning is inexpensive and, unlike synthetic bottom-up processes, it produces continuous (endless) nanofibers. Such continuous nanofibers are readily available as reinforcement in structural composites.[2] Unfortunately, the carbon nanofibers produced to date were characterized by a relatively poor graphitic structure.[38] It is well-known that improved

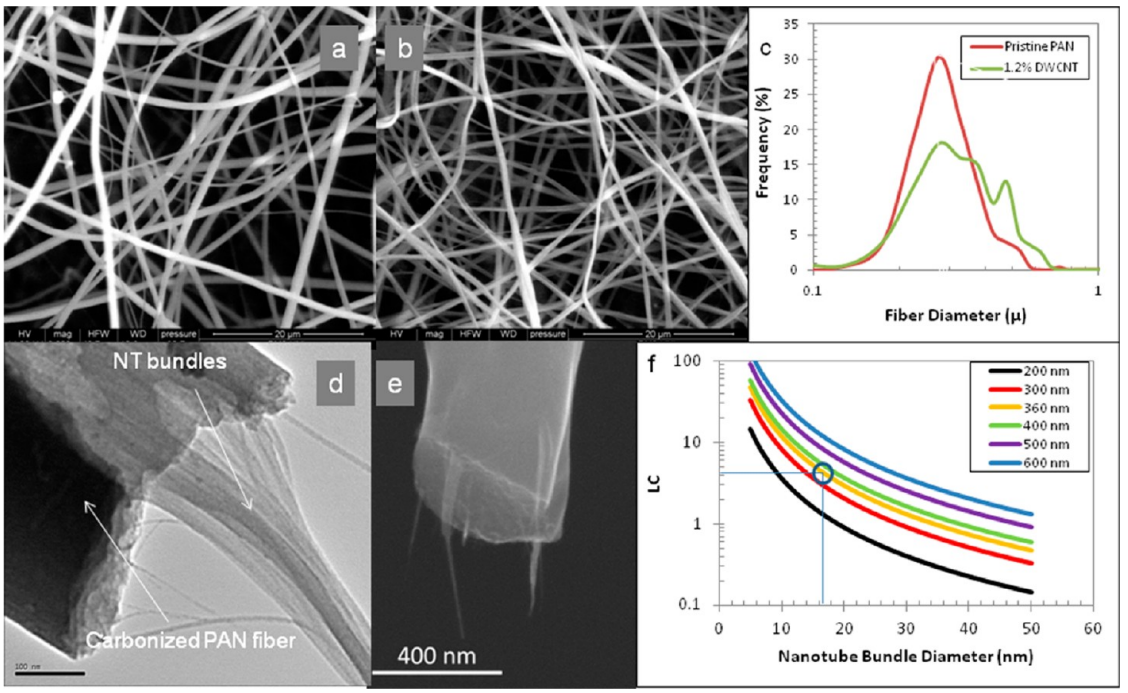

Figure 1. CNF morphology and DWNT distribution: SEM micrograph of electrospun PAN (a) and 1.2% DWNT/PAN (b) nanofibers; (c) diameter distributions for pristine PAN and 1.2% DWNT/PAN samples (as measured from approximately 200 fibers); (d) TEM micrograph of a broken edge of CNF with NT bundles; (e) SEM micrograph of the fracture surface of CNF. The pulled out DWNT bundles seemed to have uniform distribution along the length and within the cross section of the CNFs. (f) Length coverage (LC) of nanotube bundles in PAN nanofibers for different bundle and fiber diameters—the average fiber diameter measured for this sample was 360 nm and the typical bundle diameter measured was 16 nm (the corresponding point is circled).

graphitic order in carbon fibers is needed for higher elastic modulus and thermal and electrical conductivity. A degree of graphitic order and, particularly, preferential axial orientation, is also needed for higher carbon fiber strength. In this regard, CNFs are ideally suited for carbon templating. The high aspect ratio of CNFs increases nanoparticle alignment. In addition, if nanoinclusions are well-distributed over the length and within the cross-section of the nanofiber, they may initiate a global templating effect as most regions within the nanofiber will be in close proximity to inclusions.

NTs have been incorporated in electrospun nanofibers[39−43] and graphitic growth in the vicinity of nanotubes was demonstrated before.[42,43] Most earlier studies, however, were performed with multiwall carbon nanotubes (MWNTs) and the resulting CNF quality was generally poor.[39−41,43] MWNTs are more difficult to disperse and they generally have lower specific surface area. Outside the localized HRTEM observations of graphitic growth near MWNT surfaces,[42,43] there has been no systematic study of the extent and magnitude of graphitic templating using nanocarbons in CNFs.

Here we performed a coordinated experimental and theoretical study to explore the magnitude, extent, and mechanisms of graphitic structure evolution in double-wall carbon nanotube-templated CNFs. The same DWNTs as the ones used in the recent study of nanotube fibers with high NT content[26] were utilized (note that these tubes are normally present as bundles). CNFs with a small quantity of DWNTs were nanomanufactured by electrospinning, and their structure was characterized by a variety of methods. Interfacial shear strength between DWNT bundles and surrounding templated carbon was evaluated experimentally *in situ*. Initial stages of the templated carbonization process were modeled using molecular dynamics simulations on two limiting nanocarbon particle geometries. The results were analyzed and discussed in the context of commercial carbon fiber manufacturing and structure, and it was shown that well-dispersed and well-aligned carbon nanotubes can guide polymer chain orientation, while also providing an anchor to the polymer chains during carbonization. The global nature of the observed improvements in the graphitic structure and orientation in the templated CNFs shows promise as a future carbon fiber manufacturing technology.

RESULTS AND DISCUSSION

Nanofiber Morphology and NT Distribution. Figure 1 panels a and b show the overall morphology of as-spun PAN and 1.2% DWNT/PAN nanofibers. As can be seen, both pristine PAN and 1.2% DWNT/PAN samples exhibited reasonably uniform, good quality nanofibers with similar diameter distributions (Figure 1c). The

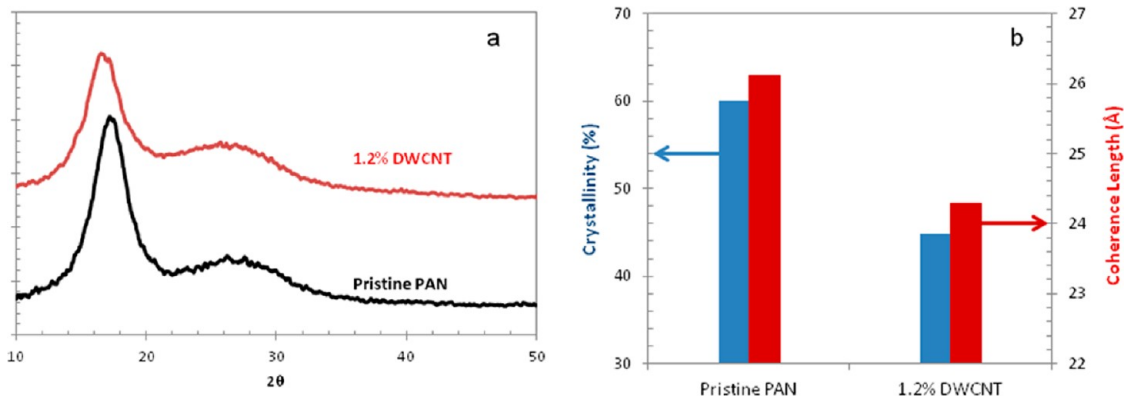

Figure 2. XRD analysis of as-spun nanofibers: (a) XRD diffractograms of neat PAN and 1.2% DWNT/PAN nanofibers; (b) computed XRD crystallinity and crystal size for neat PAN and 1.2% DWNT/PAN.

diameter distribution for the 1.2% DWNT NFs was slightly broader (after measuring approximately 200 fibers in each sample) and had a small large-diameter peak that was absent in the pristine NF sample. To examine the DWNT distribution within the nanofibers, a carbonized templated nanofiber mat was broken and examined by scanning and transmission electron microscopies (SEM and TEM). In nearly all of the several tens of fracture sites imaged, the cross sections of the nanofibers contained a few pulled out DWNT bundles (see Figure 1d,e). As seen in the Figure, the DWNT bundles were well aligned along the CNF axis.

Most CNF cross sections showed several fine DWNT bundles that appeared evenly distributed within the cross section (Figure 1e) while some exhibited slightly thicker bundles (Figure 1d). Good DWNT distribution and alignment within the CNFs correlate with their good dispersion in the solution used in electrospinning. The latter appears to be enhanced by the presence of organic functional groups on the surfaces of DWNT bundles and their favorable interaction with PAN molecules.

To determine whether or not the DWNT bundles covered the entire length of all nanofibers produced by electrospinning, we performed a theoretical calculation to estimate the length coverage, LC, of the DWNT bundles. We define the length coverage as the ratio of the total length of the nanotubes to the total length of the nanofibers. Therefore, LC > 1 means that there is on average more than one bundle of nanotubes per cross-section of the fiber. The LC of the precursor PAN nanofibers can be estimated as

$$\mathrm{LC} = \frac{\mathrm{wt_{CNT}}}{\mathrm{wt_{PAN}}} \times \left(\frac{D_{\mathrm{PAN}}}{D_{\mathrm{bundle}}}\right)^2 \times \frac{\rho_{\mathrm{PAN}}}{\rho_{\mathrm{bundle}}}$$

where D_{PAN}, D_{bundle}, ρ_{PAN}, and ρ_{bundle} are the diameters and mass densities of the PAN nanofibers and the DWNT bundles, respectively ($\rho_{\mathrm{PAN}} = 1.2$ g/cm^3, $\rho_{\mathrm{bundle}} = 1.575$ g/cm^3[326]). Figure 1f shows the expected LC for different bundle and fiber diameters. The estimated LC for the observed average bundle diameter of 16 nm and average fiber diameter of 360 nm is ~4.68. Given the thermal stability of CNTs and their encapsulation in nanofibers, the length coverage is expected to remain the same during the carbonization process (as can be seen from the micrographs, *e.g.*, Figure 1d,e, the nanotube bundles survived the carbonization process intact). Therefore, every given cross section of the bundles can be expected to be reinforced, on average, by a few bundles. This simple analysis is consistent with the fractographic investigations of CNF breaks.

Graphitic Templating at Low Carbonization Temperature. To understand the influence of polymer precursor on the CNF structure, as-spun nanofibers were analyzed by X-ray diffraction. Resulting diffractograms are shown in Figure 2a. The spectra exhibited a crystalline peak at $2\theta \approx 17.4°$ and a broad amorphous halo at approximately $2\theta \approx 26.9°$, typical of semicrystalline PAN. Note that diffraction from the small amount of DWNT is not detectable under the measurement conditions. The background was removed and the PAN crystalline peak and the amorphous halo were fitted using Lorentzian peak shapes. The polymer crystallinity was evaluated by dividing the area under the crystalline peak by the total area under the curve. The coherence length (CL, *i.e.*, "crystal size") was calculated from the width of the main crystalline peak, using the Scherrer equation:

$$\mathrm{CL\ (Å)} = \frac{K\lambda}{\beta \cos\theta} = \frac{0.9 \times 1.542}{\sqrt{(\mathrm{fwhm(Rad)}^2 - 0.002^2)}\cos\theta}$$

where shape factor (K) was taken as 0.9, the λ is the standard wavelength for a copper source, 0.002 was the instrumental peak widening calculated based on a single crystal Si standard, and θ is the Bragg angle for the crystalline peak. The results shown in Figure 2b indicate that both X-ray diffraction (XRD) crystallinity and average crystal size of PAN decreased in the presence of DWNTs.

Reduction of PAN crystallinity in the presence of DWNT can be explained by the reduced macromolecular mobility as a result of strong polymer–NT interaction, which has been observed by other researchers.[44–46]

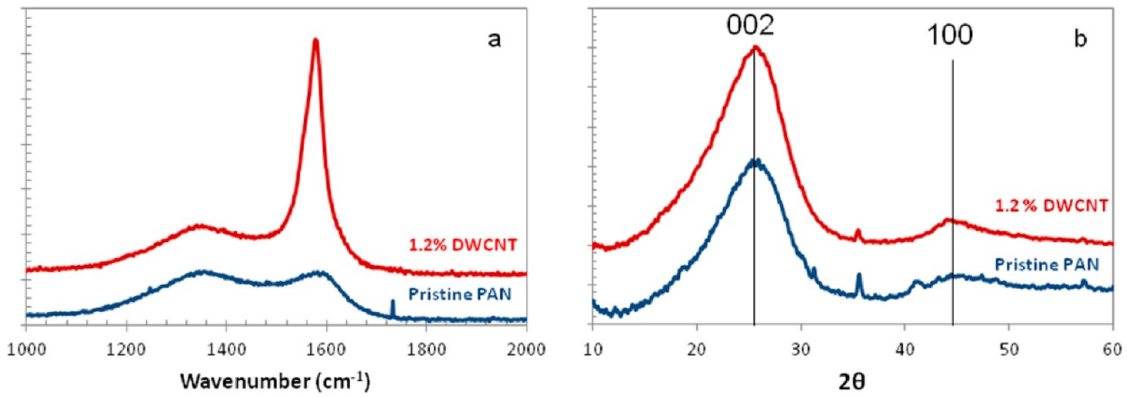

Figure 3. Structural analysis of CNFs carbonized at 800 °C: (a) Raman spectra showing significantly enhanced G band for the 1.2% DWNT sample; (b) XRD spectra for pristine PAN and 1.2% DWNT samples.

PAN crystallization could also be disrupted by the NT bundles. Reduced crystallinity results in a larger fraction of disordered or amorphous polymer chains that need to be constrained during stabilization and carbonization in order to achieve a well-ordered structure in the carbon fibers.

The graphitic structure of CNFs carbonized at 800 °C was investigated by XRD and Raman spectroscopy. First order Raman spectra of pristine and templated CNFs are shown in Figure 3a. The spectra exhibited typical behavior for carbon materials,[42] with a D band around 1358 and 1354 cm^{-1}, and G band around 1579 and 1572 cm^{-1} for the pristine and the 1.2% DWNT samples, respectively. The spectra show a significant difference in relative peak intensities as a result of the templating effect using a small amount of DWNT. Raman spectrum of the 1.2% DWNT sample showed a pronounced G band, which was significantly stronger and sharper than the one from the pristine CNFs. The spectra for the templated CNFs were compared to the Raman spectra from uncarbonized PAN/DWNT samples (not shown). The uncarbonized samples exhibited a low wavenumber shoulder in the G band as well as a general shift in the G band toward higher wavenumbers (to approximately 1592 cm^{-1}) and significantly smaller full width at half-maximum (fwhm) of the G band. These features are characteristic of a Raman signal from DWNT[47,48] and are not noticeable after carbonization, indicating that the signal from the newly formed, less perfect graphitic structures dominated the templated CNF spectrum.

The D and G bands of the carbonized samples were fitted using Lorentzian curve shapes and the integrated intensities, I_D and I_G, and the width of G band were calculated. For every nanofiber mat, an average value and standard deviation were calculated based on measurements at five different locations on the mat. Crystal structure parameters were formally extracted using the approach proposed in ref 49. The extracted parameters are shown in Table 1. The 1.2% DWNT CNF sample showed improved graphitic structure as indicated by the smaller I_D/I_G ratio and lower fwhm of the G band (see data provided in Table 1). Note, however that the spectrum for the DWNT-templated NFs included the intrinsic nanotubes' contribution that, although expected to be small, could not be separated from the overall signal of the templated CNF.

TABLE 1. Summary of Crystal Properties Extracted from XRD and Raman Spectra

	XRD			Raman		
sample	L_c (Å)	L_a (Å)	d_{002} (Å)	I_D/I_G	G band fwhm (cm^{-1})	L_a (Å)
pristine PAN	10.0	16.3	3.53	3.53 ± 0.29	110.1 ± 2.5	12.5
1.2% DWNT	10.6	28.9	3.55	1.76 ± 0.73	49.1 ± 5.4	25

CNF mats carbonized at 800 °C were also examined by XRD in the range between 2θ = 10 and 60° (Figure 3b). The diffractions showed broad 002 and 100 peaks, which became sharper for the 1.2% DWNT sample, indicating improvement in the graphitic structure. The calculated 002 spacings for both pristine and templated CNFs (Table 1) were typical for turbostratic graphite.

The crystal structure of graphite was characterized by the crystallite sizes denoted as L_c and L_a. L_c corresponds to the average crystal size perpendicular to the graphene basal planes and was calculated from the width of the 002 peak, using the Scherrer equation, while L_a corresponds to the average in-plane crystal size and was calculated from the width of the 100 peak. Analysis of the results shown in Table 1 indicates that while the L_c remained similar for both pristine PAN and 1.2% DWNT samples (~1 nm) and comprised 3−4 graphene layers, the L_a increased by almost a factor of 2 for the 1.2% DWNT sample to approximately 2.9 nm. The latter was only 25% less than the corresponding crystal size reported for the commercial carbon fiber T-300.[50] The XRD results were consistent with the Raman data.

XRD and Raman analyses of carbonized nanofibers indicate significant changes in the structure of CNFs as

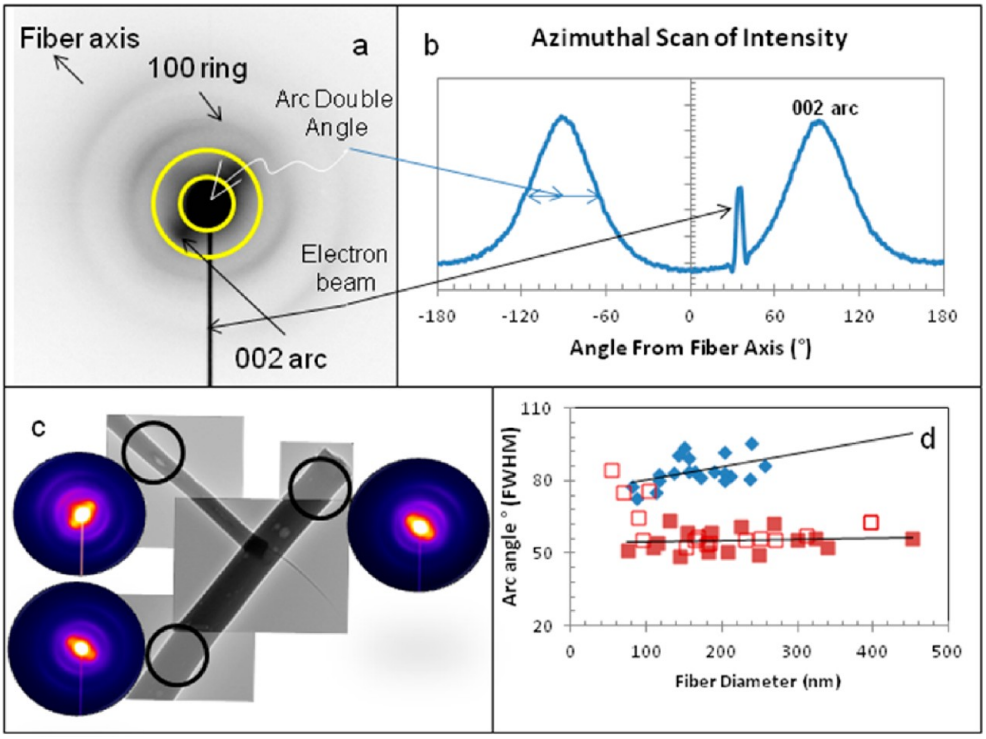

Figure 4. Selected area electron diffraction analysis of carbon nanofibers: (a) typical 2D SAED pattern; (b) azimuthal variation of scattering intensity for the 002 reflection produced by integrating the intensity of the SAED pattern between the concentric yellow circles; (c) TEM micrograph and SAED patterns from carbonized DWNT/PAN nanofibers in the areas with (top left) and without (right and bottom left) visible DWNT; (d) variations of 002 arc double angles with nanofiber diameter for carbonized pristine PAN (blue diamonds) and 1.2% DWNT sample from the areas with (full red squares) and without (empty red squares) visible NT bundles. Scale bars on panel c are 200 nm.

a result of small addition of DWNT. A comparison with the results from the as-spun polymer NFs suggests that the oriented polymer chains in the extensive amorphous PAN phase most likely were internally constrained *via* strong interactions with the DWNT bundles. These polymer chains were originally oriented by the strong extensional forces in the electrospun jets as well as by interacting with well-oriented DWNTs. However, if unconstrained, these chains would quickly lose their orientation *via* entropic shrinkage upon heating, resulting in poor graphitic structure. Such shrinkage is normally prevented during carbon fiber manufacture by applying an external stretch during stabilization and carbonization. As no such stretch was applied to the nanofibers in the case studied, the observed significant improvement of graphitic structure in the templated CNFs serves as an indicator of an internal constraint in the templated system. Such a constraint could be provided by anchoring polymer chains on the axially oriented surface of carbon nanoinclusions. Reduced polymer shrinkage and nanotube-promoted formation of a condensed aromatic ladder structure during stabilization of the NT-containing PAN fiber were also noted in refs 40,44 and 51.

Note that both Raman analysis and XRD are not localized and produce average information for nanofiber mats containing a large quantity of nanofilaments.

Selected Area Electron Diffraction (SAED) Analysis of Graphitic Structure Orientation. It is well-known that orientation of graphitic planes is crucial for good mechanical and other properties of carbon fibers. Our previous analysis of polymer and carbon nanofibers showed that their structural orientation can change as a function of nanofiber diameter. Therefore, the effect of nanofiber diameter on structure of individual DWNT-templated CNFs was investigated.

Pristine PAN and 1.2% DWNT nanofibers carbonized at 800 °C were examined in a TEM and their graphitic crystal orientation was evaluated based on electron diffraction. A typical 2D SAED pattern exhibiting 100 and 002 reflections is shown in Figure 4a. A single crystal would result in discrete points on the pattern indicative of the crystal spacing and orientation, while polycrystalline sample with randomly oriented crystallites would produce full rings. An arc indicates a polycrystalline structure with preferred orientation of the corresponding crystal plane perpendicular to the direction of the arc's maximum intensity. Analysis of the 100 rings corresponding to a family of planes perpendicular to the graphene basal planes showed weak azimuthal variation of intensity which might be the result of an anisotropic crystallite shape coupled with preferred orientation. The average intensity of the 100 reflections was weak and not analyzed in this paper. The 002 reflections, which correspond to

graphene basal planes, consisted of two pronounced arcs. This indicates that the graphitic crystals had a preferred orientation along the fiber axis. The corresponding azimuthal intensity variations, computed using the QPCED2 program,[52] are shown in Figure 4b. The width of the peaks, as illustrated in Figure 4b, indicates the degree of crystal alignment—a randomly oriented sample would have a constant intensity over the 360° angle, while a sample with highly oriented crystals would have sharp peaks and smaller arc angles.

Preferred orientation of the 002 planes along the nanofiber axis is clearly visible. The degree of this orientation, as expressed by the 002 arc double angle (from the fwhm of the peaks), was computed and plotted for the two samples as a function of nanofiber diameter (see Figure 4d). In the case of 1.2% DWNT templated CNFs, graphitic crystal orientation was examined both near the broken ends of the nanofibers with visible protruding nanotube bundles and in the areas of nanofibers where there were no visible nanotubes (Figure 4c).

As can be seen, there is a significant systematic improvement in graphitic crystal orientation in the DWNT-templated sample compared to the pristine CNFs. The orientation remained relatively constant irrespective of the nanofiber diameter for the templated sample, as opposed to the observed gradual improvement in crystal orientation with the reduction of diameter of pristine CNFs.

The fact that orientation is improved and appeared independent of CNF diameter is significant. Graphitic orientation is directly linked to carbon fiber modulus and conductivity. As mentioned above, a degree of orientation is needed for carbon fiber strength. Orientation in carbon fibers is achieved by creating and maintaining polymer chain orientation throughout the stabilization and carbonization process. Analysis of Figure 4d indicates that polymer chain orientation in pristine NFs increased as their diameter decreased. This is consistent with the extensive relevant data in the literature and our own analysis of numerous polymer NFs. Comparison with the behavior of the templated CNFs (Figure 4d) shows that the DWNTs further significantly increased initial polymer chain orientation (indicated by the dramatically improved graphitic orientation) and also made it less dependent on nanofiber diameter. The latter finding has a potential to relax the small diameter requirement for the high CNF properties that can have important manufacturing implications, as it is easier to produce larger diameter nanofibers.

Also significant is the fact that polymer chain orientation in the templated NFs translated into an improved carbon orientation without external stretch during CNF stabilization and carbonization. As mentioned earlier, the latter is considered paramount in commercial carbon fiber manufacturing. Its function is to freeze polymer orientation and prevent entropic shrinkage and loss of orientation in the disordered polymer regions during thermal treatment. Analysis of the SAED data provides additional argumentation for the hypothesis that, in the templated system, an internal constraint created by anchoring of polymer chains on the surface of oriented DWNTs has replicated, at least in part, the effect of external stretch. This may have important implications on CNF manufacturing by relaxing or even eliminating the stretch requirement during CNFs processing. The latter will be especially beneficial for the cases when stretch is difficult or impossible to apply. Examples of such cases include random or multidirectional layered NF systems and various 3D CNF architectures created by integrated single-step nanomanufacturing processes.[36]

Finally, analysis of graphitic plane orientation data from templated CNFs (Figure 4d; see filled and empty red squares) suggests that the DWNT templating effect was global, at least down to the NF diameters of approximately 100 nm. This may be the result of axial propagation of the templated graphitic growth nucleated by DWNTs or simply the consequence of good DWNT length coverage and the fact that most CNF cross sections contained one or several DWNT bundles. We believe that the latter is a more likely explanation. This argument is supported by the analysis in Figure 1f. Note that the length coverage index, LC, reduces with the decrease of CNF diameters. Local absence of NT can be the reason for several high data points in Figure 4d for the ultrafine CNFs from the areas without visible DWNTs (an indirect indication of the link between the observed templating extent and DWNT length coverage). It is worth noting, however, that the length coverage can be easily optimized by controlling DWNT concentration and/or bundle diameter. We point out that excellent solution dispersibility of DWNT in PAN/DMF and good resulting distribution of DWNTs in the electrospun NFs could be at least partially due to the beneficial organic sizing of the DWNTs produced by the floating catalyst CVD method.[26] Our experience with other NT systems often produced lower quality dispersions and nanofibers.

Overall, the combination of XRD, Raman, and SAED analyses indicates significant and global graphitic templating in the electrospun continuous CNFs containing 1.2% DWNT that were carbonized at very low temperature of 800 °C.

Effect of Carbonization Temperature. Carbonization temperature is known to be an important parameter affecting the final graphitic structure of manufactured carbons. Raman spectra for CNFs carbonized at different temperatures were collected and analyzed. The results are presented in Figure 5a,b. It is clear that the 1.2% DWNT samples exhibited better graphitic structure (as indicated by significantly reduced I_D/I_G ratio and G bandwidth) for all carbonization temperatures.

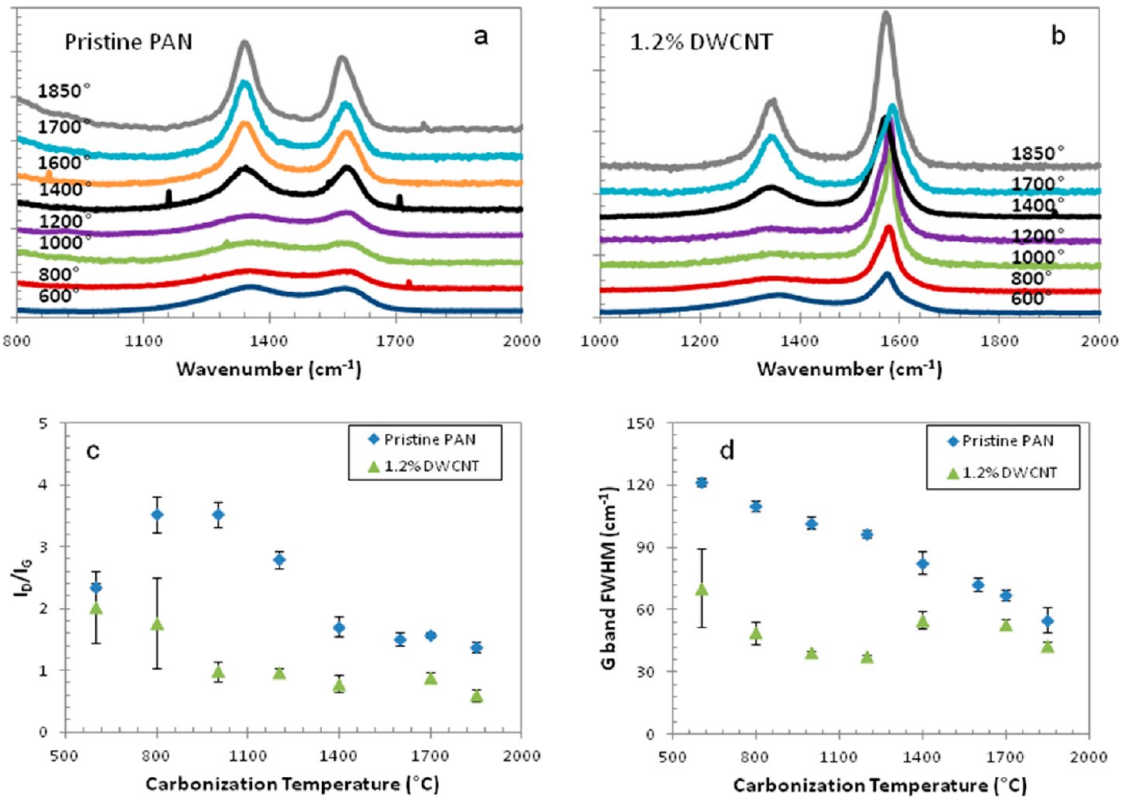

Figure 5. Analysis of the effect of carbonization temperature: (a) Raman spectra of the carbonized pristine PAN sample for different carbonization temperatures; (b) Raman spectra of the carbonized 1.2% DWNT sample for different carbonization temperatures; (c) I_D/I_G ratio as a function of carbonization temperature for both samples. The ratio is inversely proportional to in-plane graphitic crystal size L_a; (d) fwhm of G band as a function of carbonization temperature for both samples. Smaller bandwidth indicates better graphitic structure.

As expected, the graphitic structure of CNFs improved with the increase of carbonization temperature for both pristine and templated CNFs. However, it is seen that the improvement was significantly accelerated by the presence of DWNTs. Analysis of temperature variations of the extracted structural order parameters (Figures 5c,d) shows that the largest templating effect (difference between structures of templated and non-templated sample) was achieved at lower carbonization temperatures. The templating effect reaches the maximum at around 1000 °C. The level of graphitic order achieved in the templated system carbonized at 1000 °C is comparable to or better than the order in the pristine system carbonized at 1850 °C.

The above findings are significant. The increasing of carbonization temperature is a common method of improving graphitic structure of carbon materials and fibers. It has been successfully used to improve the graphitic structure of CNFs by graphitizing them at temperatures up to 3000 °C.[53] However, high temperature graphitization is expensive. The cost of the high-temperature post-treatment required to achieve high mechanical properties of the first commercial high-performance carbon fiber, Thornell by Union Carbide,[54] was a competitive disadvantage that eventually drove it out of the market. One of the main advantages of PAN-based carbon fibers is that their structure and graphitic order can be controlled by applying stretch at much lower temperatures, eliminating the need for high temperature post-treatment. Further reduction of carbonization temperature is always desirable and will further reduce the cost of carbon fiber production. Our overall data indicates that DWNT templating may simultaneously relax the stretch requirement and provide significant structural improvements at lower carbonization temperatures. Better graphitic structure and orientation are likely to result in better mechanical properties. Coupled with the possibility of achieving better structure in CNFs of larger diameters (based on recorded diameter independence of the orientation in templated CNFs discussed above) and further building on the general low cost of the top-down nanofiber manufacturing by electrospinning,[36] our results open up attractive new route for controlled ultralow-cost nanomanufacturing of high quality CNFs.

Analysis of Interfacial Interactions. Interfacial bonding is known to be very important for proper utilization of reinforcements with high mechanical properties in composites. The reinforcing effect of nanotubes at such a low volume fraction in the templated CNFs is not expected to be dramatic. However, their interfacial bonding is still important. A poor quality interface

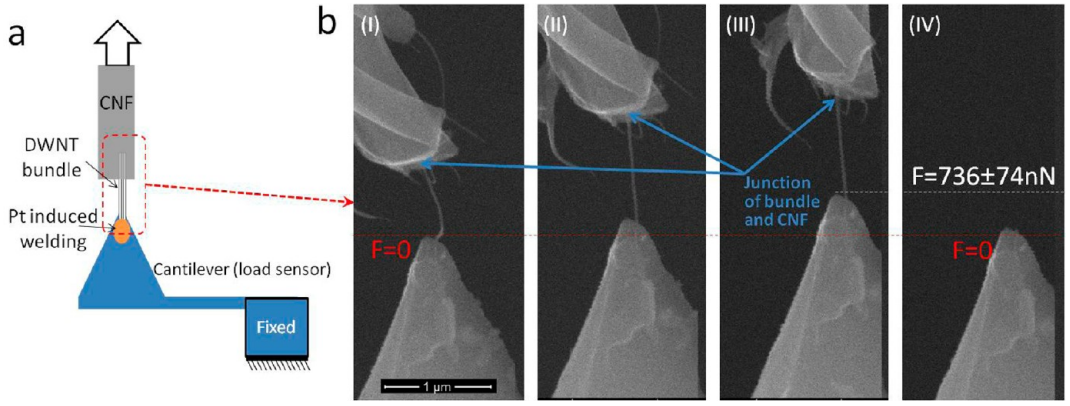

Figure 6. (a) Schematic of the experimental setup used for the *in situ* SEM investigations of the shear interactions between DWNT bundles and CNFs. (b) The sequence of steps of an attempt to induce DWNT bundle pull-out from CNFs.

between the nanotubes and the surrounding carbon matrix can introduce defects. In the absence of sufficient shear interaction in an aligned system, the DWNT bundles in CNFs will act as cylindrical voids that will adversely affect both modulus and strength.[26,55] To better understand the shear interaction between DWNT bundles and the templated carbon matrix of the CNFs, we performed a series of mechanical experiments *in situ* in an SEM. The goal of these experiments was to pull partly embedded, partly exposed DWNT bundles out of the CNFs to determine the interfacial shear strength between the two components.

The experimental setup is schematically shown in Figure 6a. A DWNT bundle, which has been pulled out from a CNF during nanofiber fracture was attached to an AFM cantilever. The latter served as the load sensor. The positioning of the CNF and AFM cantilever was facilitated by use of a nanomanipulator within an SEM chamber for visualization purposes. The pulled out DWNT bundle was attached to the AFM cantilever by e-beam induced Pt deposition. Subsequent to the bundle welding to the AFM cantilever, the CNF was pulled away from the AFM cantilever, thus a tensile axial load was developed in the bundle which tended to pull the bundle out of the CNF. The deflection of the AFM cantilever was recorded as a measure of the force in the bundle and the total interfacial shear force between the bundle and the CNF. Sequential images from a pull-out experiment are shown in Figure 6b.

In the experiment shown in Figure 6b, the DWNT bundle failed near the cantilever tip, at a true strength of ~10.3 GPa, without any detected shear failure between the bundles and the carbonized PAN, which points to strong shear interactions between the two. Several other attempts to induce pull out of the DWNT bundles further confirmed this conclusion: in all cases, DWNT bundle failure preceded a potential detachment between the bundles and the carbonized PAN, preventing the occurrence of the latter. In all cases except one, all the DWNTs of the bundles failed concurrently. In the remaining case, the outer DWNTs failed, followed by the pull out of the inner DWNTs (discussed later in this section). The results of the pull-out experiments are presented in Table 2. It is interesting to note that the measured strength of the bundles, *ca.* 4–20 GPa, was in the range of the strength of the pristine bundles reported previously,[26] suggesting that the atomic structure of the bundles has not been damaged during the carbonization. This conclusion is in line with TEM images of the bundles (Figure 1d), in which the shells of individual bundles can be observed, and also with the simulation results discussed later.

TABLE 2. Summary of the Pull-out Experiments on Templated Carbonized PAN Nanofibers

test	diameter of bundle (nm)	bundle strength (GPa)
1	13.1	10.0
2	14.2	10.3
3	15.0	>12.1[a]
4	9.6	3.9
5	12.1	20.3

[a] The sample did not fail in this case, it detached from the AFM cantilever.

Given the fact that the bundle rupture precedes shear failure of the bundle–CNF junctions, the measurement of the interfacial shear strength (IFSS) is virtually impossible. However, in a rare case (1 out of 5 experiments), we were able to estimate a lower bound for the IFSS, as shown in Figure 7. The failure observed in this case was a sword-in-sheath type failure, indicated by the sudden change in the bundle diameter, in which first the outer layer of the DWNTs of the bundle failed, followed by catastrophic pulling out of the inner DWNTs. The *post-mortem* image of the pulled out bundle is shown in Figure 7a, which is similar to what has been observed before for the DWNT bundles.[26] In this case, similar to the other cases presented here, the bond between DWNT bundles and the carbonized PAN is sufficiently strong to prevent complete detachment between the outer layer of DWNTs of the bundle and the CNF. Therefore, as the

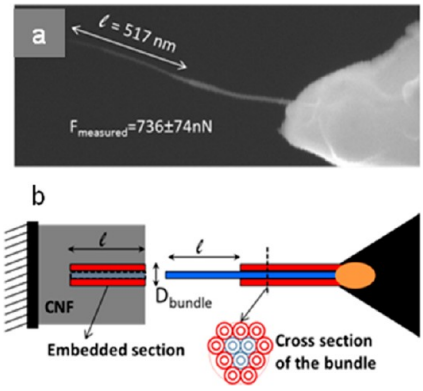

Figure 7. (a) SEM image and (b) schematic representation of one bundle that pulled out of the CNF in sword-in-sheath failure. The embedded length is shown in both panels a and b.

interface did not fail, the IFSS could not itself be measured, and must exceed the strengths measured in the pull-out experiments. However, the embedded length of the bundle, *l*, can be estimated as the length of the thinned section, as shown in Figure 7. Therefore, a lower bound for the average IFSS (referred to as $IFSS_{LB}$) can be estimated as

$$F_{\text{interface failure}} \geq F_{\text{measured}} \Rightarrow \text{IFSS} = \frac{F_{\text{interface failure}}}{\pi D_{\text{bundle}} l} \geq \frac{F_{\text{measured}}}{\pi D_{\text{bundle}} l} = \text{IFSS}_{\text{LB}}$$

where $F_{interface\ \ failure}$ and $F_{measured}$ are the forces required to break the junction between the bundle and the carbonized PAN, and the maximum force measured during the pull out attempts.

Given $F_{\text{measured}} \approx 736 \pm 74$ nN, with the embedded length of ~517 nm and the bundle diameter of ~14 nm, the average $IFSS_{LB}$ is estimated to be $\sim 32 \pm 3$ MPa. This lower bound to the shear strength is higher than the values predicted by pure van der Waals (vdW) interactions, pointing to the presence of stronger interactions between the NTs and the carbonized PAN, such as $\pi-\pi$ interactions between DWNTs and the graphitized regions of the CNF and/or low density of covalent bonds[56−58] and is more consistent with interfacial strength measured in NT/polymer pull-out experiments[59] for significantly smaller embedding lengths. This value is also comparable to typical epoxy/carbon interfacial strengths[60] of 30−80 MPa. Overall, the good interfacial bonding observed in our experiments is consistent with the strong templating effects described above.

ReaxFF Molecular Dynamics Simulations of Initial Stages of Templated Carbonization. In this section molecular dynamics simulations with a reactive force field are used to study the initial stages of the templated carbonization process. Experimental observation of the complex concurrent 3D propagating chemical reactions involved in carbonization is currently impossible, and the simulations are limited by system size and stimulation duration that is feasible to study, so only qualitative connections between theory and experiment are possible. However recent molecular dynamics simulations of the initial stages of carbonization in a stabilized PAN structure[61] have proven useful for understanding the reaction mechanisms that lead to carbonization, including the effects of temperature and density on the rates of graphitic structure formation. Here, this modeling approach is further expanded and used to simulate the effects of templates.

Currently, it is computationally not feasible to simulate the exact geometry of a DWNT bundle surrounded by the stabilized PAN molecules. We have therefore simulated and compared two limiting geometries, that is, a small diameter cylindrical single wall nanotube (SWNT) and a flat graphene nanoparticle. The actual case of the DWNT bundles considered here will fall in between these selected limiting geometries.

As discussed above, a well-oriented stabilized PAN precursor structure is crucial for good quality carbon fibers. Our experimental analysis indicates that such orientation exists and may be preserved in the templated NFs with the help from anchoring polymer molecules on the axially oriented templating particles. This preexisting orientation was modeled in the analysis below by aligning the initial ladder polymer precursor molecules along the particle surface or axis.

The simulations were performed using the ReaxFF[62] force field. ReaxFF uses a general relationship (i) between bond distance and bond order and (ii) between bond order and bond energy—allowing for proper dissociation of bonds to give separated atoms. Other valence terms (angle and torsion) are defined in terms of the same bond orders so that all these terms go to zero smoothly as the bonds break. It has been demonstrated in the literature that ReaxFF is suitable to study various reactions for systems consisting of C, N, O, and H atoms.[63−66] In another paper, we have studied the carbonization of PAN alone using molecular dynamics based on ReaxFF, and the results are consistent with known properties of the carbonization process in terms of gaseous species emitted during the process, and the types of structures that are produced, subject to constraints of the simulations that require us to use higher temperatures than in the experiments, and very short simulation times such that the carbonization process is only partially completed.[61]

As in the earlier work, we have assumed that the molecule ($C_{32}H_{14}N_{10}$), denoted B in Figure 8a and 8e, is the species produced by stabilization, and therefore is the starting point in the carbonization simulation. Morita *et al.* have demonstrated that this is likely to be 30% of the structure formed from PAN during stabilization,[67] and in the present study we assume that this is also appropriate in the presence of NT or graphene. For simulations involving the composite

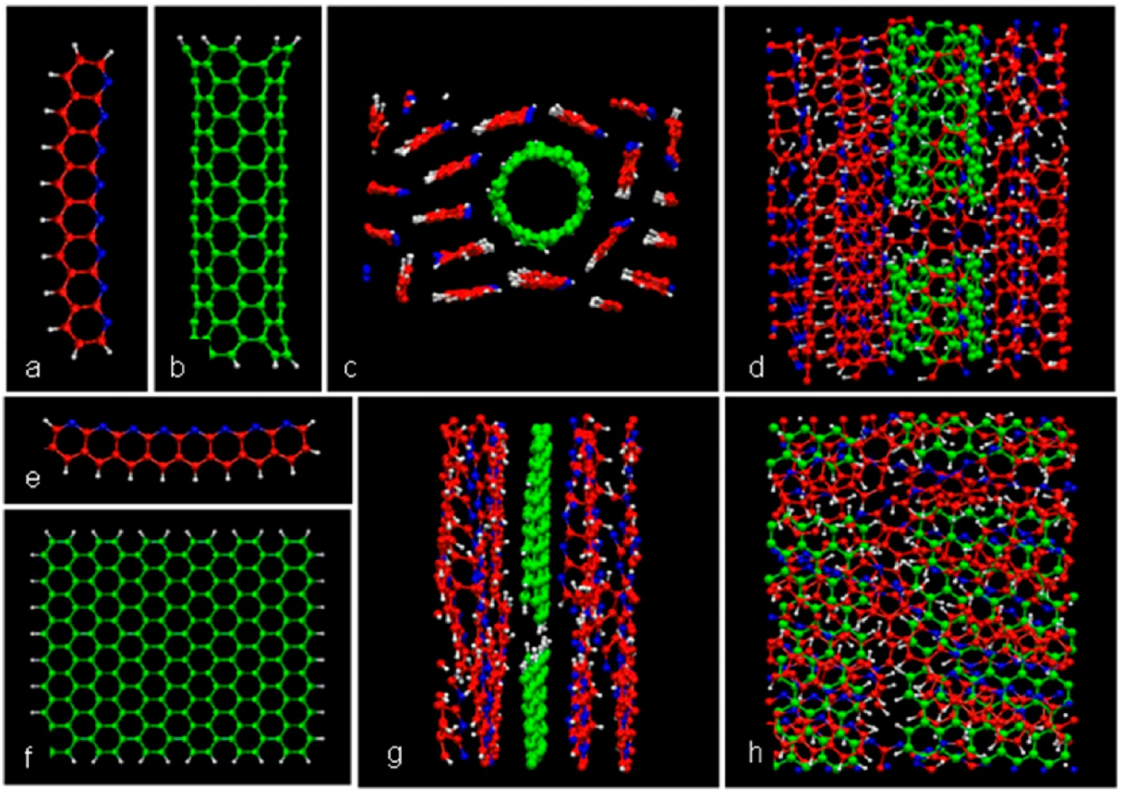

Figure 8. MD models with NT and graphene particles. (a) Model stabilized PAN molecule B; (b) SWNT (5,5) of length 22 Å. Snapshots at 50 ps of the model equilibrated at 300 K: (c) view along SWNT axis; (d) view perpendicular SWNT. (e) Model stabilized PAN molecule B; (f) graphene sheet. Snapshots at 50 ps of the model equilibrated at 300 K: (g) view along parallel to graphene sheet; (h) perpendicular view. Color code: Carbon atoms on B molecules are represented by red and on graphene and on CNT by green spheres. Nitrogen and hydrogen atoms are represented by blue and white spheres, respectively.

systems, we have compared the systems consisting of B (stabilized PAN) plus single wall carbon nanotube (SWNT) or B (stabilized PAN) plus graphene. The SWNT and graphene sheet were assumed to be finite structures, and therefore were hydrogen terminated. The uncapped SWNT is taken to have the chirality (5, 5), radius of 3 Å and length of 22 Å. The graphene sheet is taken to have the dimensions 22 Å by 29 Å. In accordance with the experimental discussion above, the B molecules in both models were axially aligned with the presumed CNF axis and were parallel to the initial SWNT axis or graphene plane, respectively. The two model systems consist of (1) 16 B molecules and a single CNT (with 190 carbon and 20 hydrogen atoms), thus consisting of 21 wt % CNT, and (2) 16 B molecules and a single graphene sheet (with 204 carbon and 40 hydrogen atoms) thus consisting of 23 wt % graphene. Obviously the CNT or graphene content is much higher than in the experiments, a limitation associated with the required small simulation size; however, there is no suggestion in our calculations that it perturbs the carbonization process to be different from that of a much smaller concentration simulation. Periodic boundary conditions were applied in all directions of the simulation cell. The size of the simulation cell was adjusted such that the initial density was 1.60 g/cm^3 or 1.75 g/cm^3 at 300 K in case of PAN + CNT composite system. In case of PAN + graphene the initial densities were 1.6 g/cm^3 or 1.8 g/cm^3. These density choices are within the range of reported densities during carbon fiber production to form PAN.[68,69]

The model systems were equilibrated at 300 K for 60 ps as the first step of the calculations. The initial structures and snapshots of 300 K equilibrated composite structures with CNT and graphene are shown in Figure 8.

For the annealing simulation 10 structures were collected from this equilibration trajectory during the time interval 50 to 60 ps. The resulting trajectories are denoted as BG2500K_dx_*n* and BNT2500K_dx_*n*, where x = 1 and 2, and n = 1 to 10. Here d1 and d2 corresponds to the two choices of initial densities of the composite systems. The systems were then annealed up to 3000 K at a rate of 10 K/ps. Upon analyzing these trajectories no reaction or growth was observed until the temperature was raised to 2500 K or above. In view of this (which is consistent with what was found in the pure PAN simulations[61] and reflects the conditions needed to study carbonization on a short time scale), we assumed that the carbonization step involved canonical (NVT molecular dynamics) annealing conditions, and in the simulations used a constant temperature of 2500 K for 500 ps. During these constant temperature simulations volatile gases such as

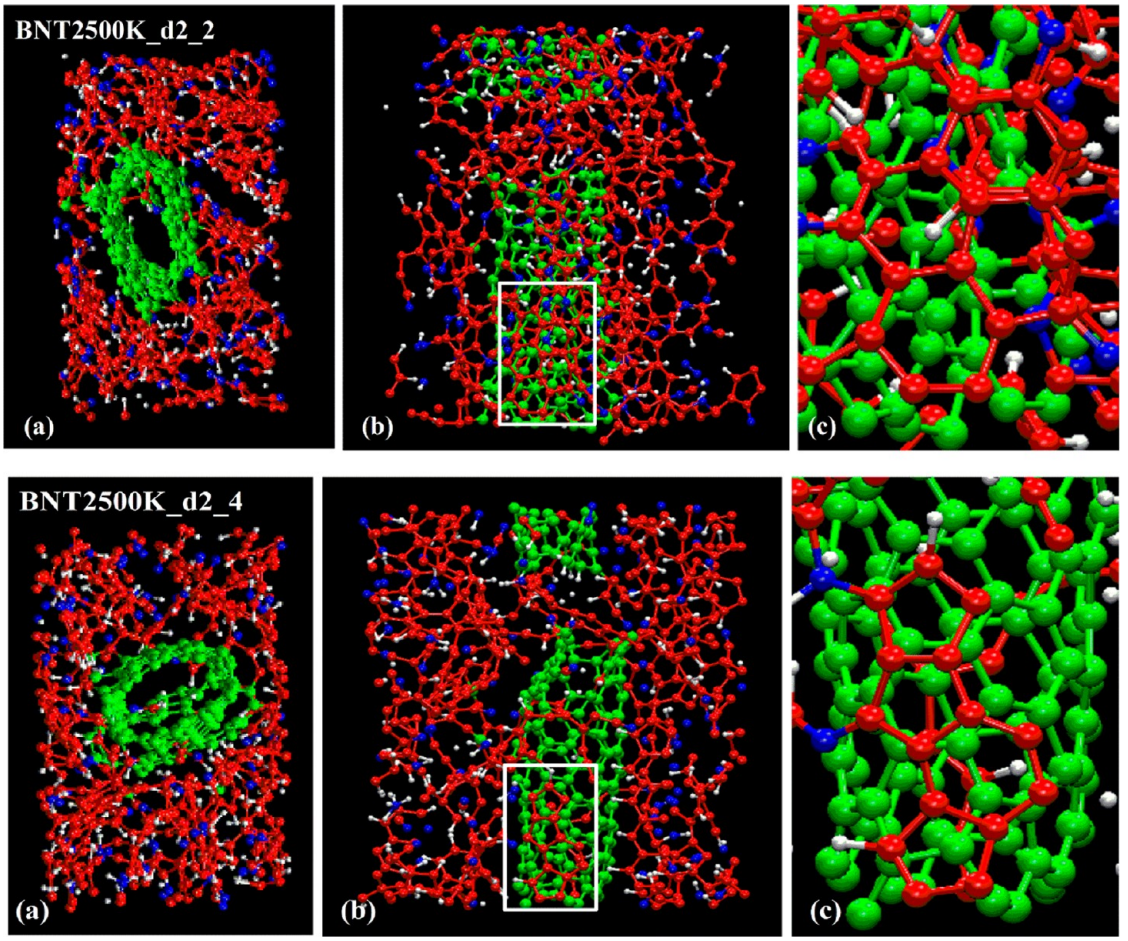

Figure 9. Snapshots at 500 ps for CNT composite system: (a) view along CNT axis; (b) view perpendicular CNT axis; (c) detailed view of selected part. Color code: Carbon atoms on B molecules and on graphene are represented by red and green spheres, respectively. Nitrogen and hydrogen atoms are represented by blue and white spheres, respectively.

N_2, H_2, HCN, and NH_3 were removed from the system at every 50 ps to emulate the removal of these gases in the experiments. The trajectories were analyzed during the course of simulations by estimating the number and type of gaseous species evolved, the number and composition of rings broken or formed, the hybridization of the carbon atoms, the carbon content in the growing structure, elementary reactions of small species formed during the process and the formation and growth mechanism of sp^2-type carbon structures.

The analysis below summarizes the main templating effects. The molecular dynamics calculations show that breaking of the heterocyclic rings starts to occur ~2500 K and subsequently small volatile molecules, like N_2, H_2, HCN, and NH_3, are formed as well as new π-conjugated carbon clusters consisting of five, six, and seven-membered carbon-only rings. Representative snapshots at 500 ps showing fused five- and six-membered rings structures are shown in Figure 9 for the SWNT composite system and Figure 10 for the graphene composite. The upper panel of Figure 9 shows the formation of five six-membered rings, whereas the lower panel shows the formation of three five-membered rings and one six-membered ring. Similarly the upper panel of Figure 10 shows the formation of two five-membered rings and a six-membered ring and the lower panel shows the formation of three six-membered rings. Further ring condensation and growth occurs around these clusters (*i.e.*, these clusters serve as nuclei for further carbonization).

The populations of small molecule species formed during the simulations, averaged over 10 trajectories, are shown in Supporting Information (SI) Figure S1. The analysis shows that the formation of N_2 and H_2 is more likely than NH_3 and HCN, with N_2 formation initiating earlier than H_2 formation. N_2 formation occurs *via* three distinct stages as observed in these simulations: (i) CN-bond breaking—where original six-membered heterocyclic rings break, (ii) NN-bond formation—N with dangling bond reacts with another N of a neighboring molecule, and finally (iii) subsequent CN-bond breaking helps to form N_2.

The populations of newly formed rings consisting of carbon atoms only are shown in Figure 11. In general five-membered ring formation occurs first as a result of N_2 formation in which the six-membered heterocyclic

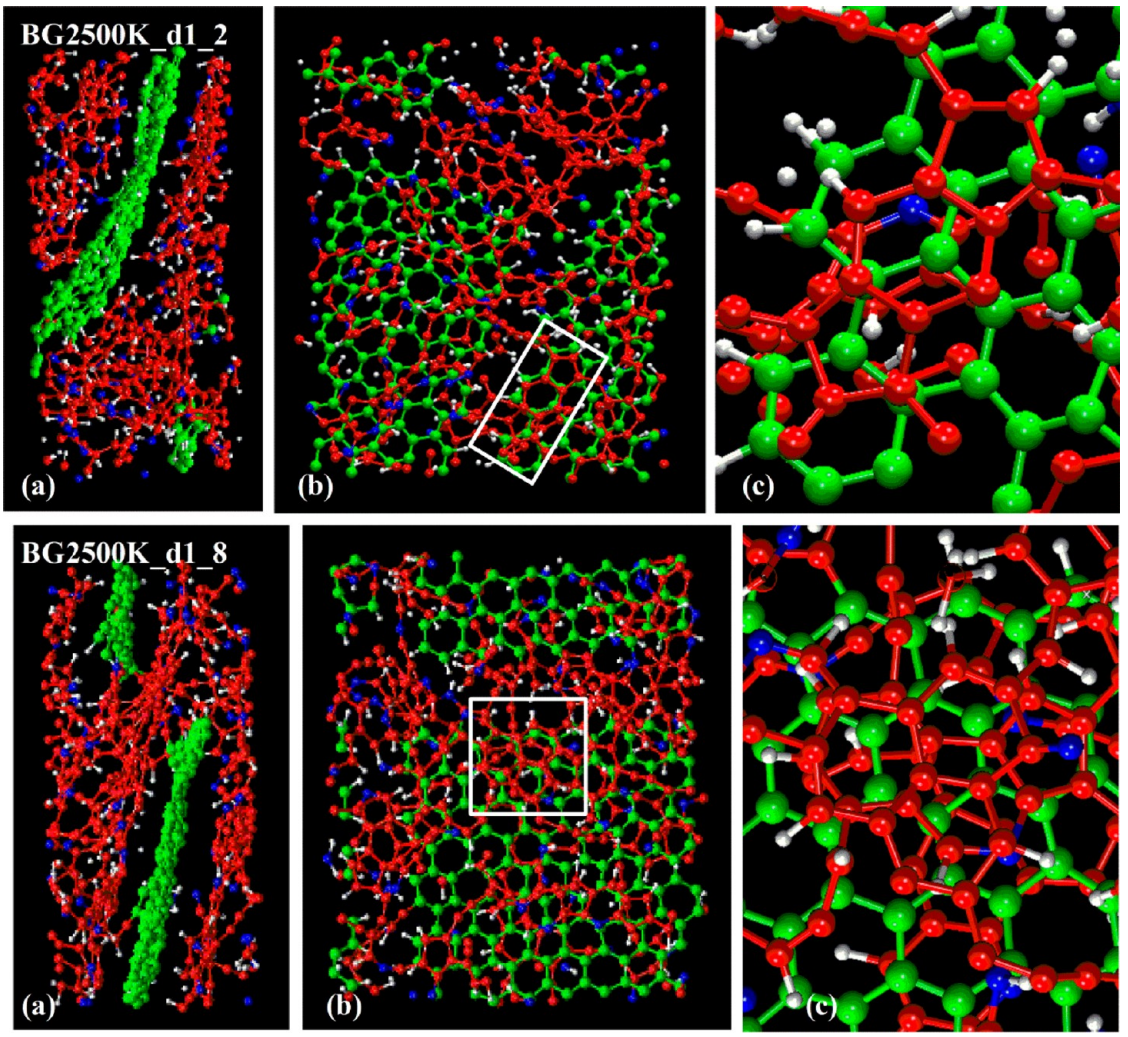

Figure 10. Snapshots at 500 ps for graphene composite system: (a) view parallel to graphene plane; (b) perpendicular view; (c) detailed view of selected part. Color code: Carbon atoms on B molecules and on graphene are represented by red and green spheres, respectively. Nitrogen and hydrogen atoms are represented by blue and white spheres, respectively.

rings of the seed molecules break and the carbon atoms in the same PAN(B) unit with dangling bonds in the newly formed structures react to form five-membered rings. Initially five-membered ring formation is dominant but in later stages of growth six-membered ring formation also becomes prominent. Conversion of five- and seven-membered rings into six-membered rings is observed, and thus the most stable π-conjugated structures are formed. It is to be noted that the formation of five-membered rings in the mechanism of carbonization is not usually considered in carbonization mechanisms but is an obvious outcome of our simulations.

The formation rate of small molecules and new rings consisting of carbon atoms only are shown in Supporting Information, Table S1 and Table 3, respectively. Note that these rates are based on results present after 500 ps and do not reflect shorter time-scale effects. Results for the PAN(B) only model are presented elsewhere.[61] So here we concentrate on the effect of templating on the results. The analysis shows that the N_2 and NH_3 formation rates are much higher for the pure PAN(B) model than for the PAN(B) + graphene model while the rates for the PAN(B) + CNT model are intermediate between the other models except for HCN. In the case of new ring formation, the six-membered ring formation rate is much higher in case of the PAN(B) model, while the five-membered and seven-membered ring formation rates are higher in the case of the PAN(B) + CNT model. The formation rate of new six-membered rings is very low for the PAN(B) + CNT model.

As stated above, initially structures consisting of five- and six-membered rings are formed. Short polyyne-like structures (with carbon atoms in the backbone) are formed due to ring breaking and N_2 and H_2 formation. These short polyyne-like structures may entangle themselves to form new five-, six- and seven-membered rings consisting of carbon atoms only. Once a small cluster consisting of five- and/or six-membered rings forms it acts as a nucleus, and further ring condensation occurs around it. The newly

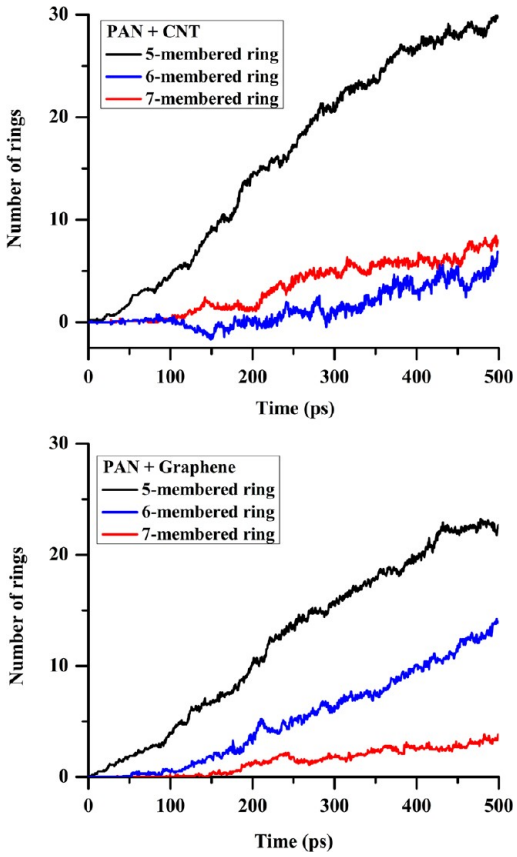

Figure 11. Number of rings formed (consisting of carbon atom only) during simulations at 2500 K and with a density of 1.6 g/cm^3. Values averaged over 10 trajectories.

TABLE 3. Ring (Consisting of Carbon Atoms Only) Formation Rate (number of rings/ns) for Simulations at 2500 K and Density of 1.6 gm/cc. Values averaged over 10 Trajectories

model	five-membered ring	six-membered ring	seven-membered ring
PAN	57.5	43.5	9.0
PAN + CNT	59.6	13.6	15.8
PAN + graphene	44.9	26.9	6.7

formed initial structures consisting of five- and six-membered rings on different units may also react among themselves to form larger structures consisting of five- and six-membered rings with carbon atoms in the backbone. Thus, three-dimensional structures consisting of five- and six-membered rings and mainly sp^2-carbon are formed. Upon continued annealing the five- and seven-membered rings may convert to more stable six-membered rings. Thus, from the present ReaxFF simulations the following distinct stages were observed in the carbonization mechanism (both with pure PAN and with the PAN+CNT and PAN + graphene composite systems): (i) formation of small structures consisting of five- and six-membered carbon-only rings *via* N_2 evolution, (ii) ring condensation, that is, further ring formation due to entanglement of small sp-type carbons (polyynes) that become attached to the five- and six-membered rings, (iii) cluster growth—small carbon-only ring clusters on different units react to form larger ring clusters, with formation of H_2, HCN, NH_3, and other species continuously occurring.

In the case of simulations with the PAN + graphene composite system, the five- and six-membered rings are predominantly formed parallel to the plane of the graphene sheet, which is a direct effect of the template. This is apparent in Figure 10, where layers of newly formed rings are clearly visible immediately on either side of the graphene layer. This result is also consistent with past experiments involving MWCNTs.[42,43] In some cases, more than one π-conjugated layer is formed, all being parallel to the graphene sheet. In case of the SWNT composite system, no cylindrically curved graphitic planes are observed (Figure 9). This can be understood as arising because the (5, 5) CNT diameter is too narrow to support templating. The experiments in refs 42,43 have been done with large diameter MWNTs, so our studies of graphene (which can be considered as a CNT with a very large diameter) composite system may be more representative of the large diameter MWNT-templating during carbon nanofiber production. Importantly, in both composite systems studied, there was a distinct preferred axial orientation of the planes of the newly formed rings and the early stacks. This is consistent with the experimental results described here and demonstrates how both the presence of the oriented carbon particles and the initial orientation of the stabilized PAN molecules (also influenced by the templating particles *via* internally constrained stabilization, as discussed above) result in improved orientation of the graphitic structure in the templated CNFs.

Additional insight into these results is provided in the Supporting Information, where we show radial distribution functions as a function of the distance from the graphene or CNT and carbon atoms that are in the pure carbon-containing rings. These results show that with one exception, a separation distance is in the range 3.0−3.5 Å that is typical for spacing between graphitic sheets, and there are no carbon−carbon covalent bonds between the graphene or CNT and the surrounding carbon-containing rings. The overall simulation results are consistent with the experimental observations. In particular, the observed preferred axial orientation of the planes of the newly formed rings in the two limiting geometric cases considered here indicates that the improved orientation effect is general and should be observed on all intermediate template geometries.

SUMMARY AND CONCLUSIONS

In summary, good quality PAN/1.2% DWNT nanofibers were produced from PAN/DWNT solutions by electrospinning. Nanofiber quality and uniformity were

significantly better than that of typical NT-modified NFs reported in the literature (the majority of past reports were using MWNTs). DWNT bundles were found to be present in most CNF cross sections and were well aligned along the CNF axis. The incorporation of a small amount of DWNT was shown to have a dramatic effect on the graphitic structure and crystal orientation of the carbonized CNFs. The templating effect was most significant at lower carbonization temperatures, leading to graphitic quality in the templated system carbonized at 1000 °C being on par with the quality of pristine CNFs carbonized at 1850 °C. Incorporation of DWNT led to a significantly improved orientation of graphitic structure that was, in addition, less diameter-dependent (in the range of CNF diameters studied). Several experimental indicators show that the templating effects were global, meaning the graphitic structure propagated from the DWNT templates to the surrounding CNF material. *In situ* SEM studies of interfacial interactions showed good bonding between DWNT bundles and the templated carbon matrix. Molecular dynamics simulations confirmed the templating and preferred orientation effects and provided additional insights into initial stages of templated carbonization.

Overall, the results of this work suggest a new inexpensive route to manufacture continuous nanofibers with improved structure and properties. The low cost is assured by economical top-down nanomanufacturing, the possibility of lower carbonization temperature, relaxed requirements on stretch during nanofiber stabilization and carbonization, and possible increase of useable nanofiber diameters.

METHODS

DWNTs were produced in a CVD process utilizing a floating catalyst system based on ferrocene and ethyl alcohol as a hydrocarbon feedstock. The as-produced DWNTs comprised up to 13 wt % of organic compounds dominated by substituted acrylates ("sizing").[26] The DWNTs were partially purified and organic sizing content was reduced to 5 wt %. In addition to organic sizing, the partially purified DWNT contained 5.4 wt % of Fe, 4 wt % of amorphous C, and 1 wt % of graphite. The DWNT content was 85 wt %. The DWNTs were considerably longer than the commercially available nanotubes (above 50 μm). Their unique organic sizing allowed for stable dispersions in polar solvents.

DWNTs were dispersed in dimethylformamide (DMF) using high speed shear mixing at 17500 rpm for 6 h. PAN polymer (Pfaltz and Bauer, Inc.; cat no. P21470, MW 150 000) was then added and fully dissolved to produce a 10%PAN/0.12%DWNT wt/wt dispersion in DMF. The dispersion underwent ultrasonication in an ultrasonic bath for 1.5 h and the quality of the dispersion was examined in an optical microscope. The above weight ratio resulted in 1.2% weight fraction of DWNT in PAN nanofibers after electrospinning. Note that the DWNT weight fraction in carbonized nanofibers is higher due to the weight loss of PAN during oxidation and carbonization. The exact weight loss is unknown, therefore, for simplicity, both PAN and carbon nanofibers containing DWNT were labeled as 1.2% DWNT nanofibers.

Nanofibers were electrospun at 12 kV using a 0.6 mL/h feed rate and a 20 ga needle. The spinneret-collector distance was 20 cm. Templated polymer and carbon nanofibers were compared with pristine PAN and carbon NFs produced under similar conditions (10 wt %/wt solution of PAN in DMF). As-spun nanofibers were examined by FE SEM (FEI Quanta 200FEG) and analyzed by wide-angle X-ray diffraction (WAXD) using Rigaku multiflex X-ray diffractometer with Cu Kα radiation in the range of 2θ between 10 and 50 degrees.

As-spun nanofibers were converted to carbon nanofibers using known protocols.[38] Nanofiber mats were stabilized in oxygen atmosphere at 270 °C for 1 h and carbonized at several carbonization temperatures in different environments. Carbonization at temperatures between 600 and 1200 °C was performed in nitrogen; carbonization at 1400 and 1600 °C was performed in argon; and carbonization at 1700 and 1850 °C was performed in vacuum. All carbonization processes used a heating rate of 10°/min and dwell time of 1 h.

The graphitic structure of the carbonized samples was evaluated by inVia Raman microscope from Renishaw using 514 nm laser as an excitation source. First order Raman spectra (1000−2000 cm^{-1}) were recorded at a resolution of 1.68 cm^{-1}. Each CNF mat was examined in five different locations to produce average values and standard deviations for the G bandwidth and the I_D/I_G ratios. Fiber mats carbonized at 800 °C were also examined by WAXD. The carbonized nanofibers were examined in a JEM 2010 transmission electron microscope from JEOL and 002 crystal plane orientations were evaluated using select area electron diffraction (SAED) from azimuthal scans as a function of nanofiber diameter.

Interfacial bonding between the DWNT bundles and surrounding templated matrix was studied by pull-out experiments. The experiments were performed *in situ* in an SEM chamber. The exposed end of embedded DWNT bundles were welded to a cantilever, and the applied load was calculated from the continuously observed cantilever deflection.

Modeling of the initial stages of templated carbonization was performed using reactive force field (ReaxFF) molecular dynamics (MD) simulations. The simulations traced the evolution of the polymer molecular structure, small molecular species, and carbon ring formation for two cases of templating carbon geometries, that is, small diameter nanotubes and flat graphene particles (as an approximation to the surface of a bundle). Further details of the simulations are presented in the text.

Conflict of Interest: The authors declare no competing financial interest.

Acknowledgment. This work was supported in part by the ARO MURI award W911NF-09-1-0541, NSF awards NIRT-0709333, CMMI-0600675, and CBET-1140065 and AFOSR award FA9550-11-1-0204. The authors thank Dr. Xingzhong Li, Nebraska Center for Materials and Nanoscience for the use of QPCED2 program. G.C.S. and B.S. are thankful to Dr. Adri van Duin, Pennsylvania State University, United States, for the use of the ReaxFF program and his help. The Quest computer system at Northwestern University was used for MD simulations.

Supporting Information Available: (1) MD simulation of evolution of small molecular species during templated carbonization; (2) radial distribution functions as a function of the distance from the graphene or CNT and carbon atoms that are in the pure carbon-containing rings. This material is available free of charge *via* the Internet at http://pubs.acs.org.

REFERENCES AND NOTES

1. Van Noorden, R. The Trials of New Carbon. *Nature* **2011**, *469*, 14–16.
2. Dzenis, Y. A. Structural Nanocomposites. *Science* **2008**, *319*, 419–420.
3. Ritchie, R. O. The Quest for Stronger, Tougher Materials. *Science* **2008**, *320*, 448.

4. Ajayan, P. M.; Tour, J. M. Materials Science: Nanotube Composites. *Nature* **2007**, *447*, 1066–1068.
5. Chae, H. G.; Sreekumar, T. V.; Uchida, T.; Kumar, S. A Comparison of Reinforcement Efficiency of Various Types of Carbon Nanotubes in Polyacrylonitrile Fiber. *Polymer* **2005**, *46*, 10925–10935.
6. Vaisman, L.; Larin, B.; Davidi, I.; Wachtel, E.; Marom, G.; Daniel Wagner, H. Processing and Characterization of Extruded Drawn MWNT-PAN Composite Filaments. *Composites, Part A* **2007**, *38*, 1354–1362.
7. Chen, W.; Tao, X.; Liu, Y. Carbon Nanotube-Reinforced Polyurethane Composite Fibers. *Compos. Sci. Technol.* **2006**, *66*, 3029–3034.
8. Li, Y.; Yu, T.; Pui, T.; Chen, P.; Zheng, L.; Liao, K. Fabrication and Characterization of Recyclable Carbon Nanotube/Polyvinyl Butyral Composite Fiber. *Compos. Sci. Technol.* **2011**, *71*, 1665–1670.
9. Chae, H. G.; Minus, M. L.; Kumar, S. Oriented and Exfoliated Single Wall Carbon Nanotubes in Polyacrylonitrile. *Polymer* **2006**, *47*, 3494–3504.
10. Mikolajczyk, T.; Szparaga, G.; Bogun, M.; Fraczek-Szczypta, A.; Blazewicz, S. Effect of Spinning Conditions on the Mechanical Properties of Polyacrylonitrile Fibers Modified with Carbon Nanotubes. *J. Appl. Polym. Sci.* **2010**, *115*, 3628–3635.
11. Vigolo, B.; Pénicaud, A.; Coulon, C.; Sauder, C.; Pailler, R.; Journet, C.; Bernier, P.; Poulin, P. Macroscopic Fibers and Ribbons of Oriented Carbon Nanotubes. *Science* **2000**, *290*, 1331–1334.
12. Vigolo, B.; Poulin, P.; Lucas, M.; Launois, P.; Bernier, P. Improved Structure and Properties of Single-Wall Carbon Nanotube Spun Fibers. *Appl. Phys. Lett.* **2002**, *81*, 1210–1212.
13. Young, K.; Blighe, F. M.; Vilatela, J. J.; Windle, A. H.; Kinloch, I. A.; Deng, L.; Young, R. J.; Coleman, J. N. Strong Dependence of Mechanical Properties on Fiber Diameter for Polymer/Nanotube Composite Fibers: Differentiating Defect from Orientation Effects. *ACS Nano* **2010**, *4*, 6989–6997.
14. Ericson, L. M.; Fan, H.; Peng, H.; Davis, V. A.; Zhou, W.; Sulpizio, J.; Wang, Y.; Booker, R.; Vavro, J.; Guthy, C.; *et al.* Macroscopic, Neat, Single-Walled Carbon Nanotube Fibers. *Science* **2004**, *305*, 1447–1450.
15. Davis, V. A.; Parra-VasquezA, N. G.; Green, M. J.; Rai, P. K.; Behabtu, N.; Prieto, V.; Booker, R. D.; Schmidt, J.; Kesselman, E.; Zhou, W.; *et al*. True Solutions of Single-Walled Carbon Nanotubes for Assembly into Macroscopic Materials. *Nat. Nanotechnol.* **2009**, *4*, 830–834.
16. Li, Y.; Kinloch, I. A.; Windle, A. H. Direct Spinning of Carbon Nanotube Fibers from Chemical Vapor Deposition Synthesis. *Science* **2004**, *304*, 276–278.
17. Koziol, K.; Vilatela, J.; Moisala, A.; Motta, M.; Cunniff, P.; Sennett, M.; Windle, A. High-Performance Carbon Nanotube Fiber. *Science* **2007**, *318*, 1892–1895.
18. Boncel, S.; Sundaram, R. M.; Windle, A. H.; Koziol, K. K. K. Enhancement of the Mechanical Properties of Directly Spun CNT Fibers by Chemical Treatment. *ACS Nano* **2011**, *5*, 9339–9344.
19. Jiang, K.; Li, Q.; Fan, S. Nanotechnology: Spinning Continuous Carbon Nanotube Yarns. *Nature* **2002**, *419*, 801–801.
20. Dalton, A. B.; Collins, S.; Munoz, E.; Razal, J. M.; Ebron, V. H.; Ferraris, J. P.; Coleman, J. N.; Kim, B. G.; Baughman, R. H. Super-Tough Carbon-Nanotube Fibres. *Nature* **2003**, *423*, 703–703.
21. Zhang, M.; Atkinson, K. R.; Baughman, R. H. Multifunctional Carbon Nanotube Yarns by Downsizing an Ancient Technology. *Science* **2004**, *306*, 1358–1361.
22. Zhang, X.; Jiang, K.; Feng, C.; Liu, P.; Zhang, L.; Kong, J.; Zhang, T.; Li, Q.; Fan, S. Spinning and Processing Continuous Yarns from 4-Inch Wafer Scale Super-Aligned Carbon Nanotube Arrays. *Adv. Mater.* **2006**, *18*, 1505–1510.
23. Zhang, X.; Li, Q.; Holesinger, T. G.; Arendt, P. N.; Huang, J.; Kirven, P. D.; Clapp, T. G.; DePaula, R. F.; Liao, X.; Zhao, Y.; *et al.* Ultrastrong, Stiff, and Lightweight Carbon-Nanotube Fibers. *Adv. Mater.* **2007**, *19*, 4198–4201.
24. Zhang, S.; Zhu, L.; Minus, M.; Chae, H.; Jagannathan, S.; Wong, C.; Kowalik, J.; Roberson, L.; Kumar, S. Solid-State Spun Fibers and Yarns from 1-mm Long Carbon Nanotube Forests Synthesized by Water-Assisted Chemical Vapor Deposition. *J. Mater. Sci.* **2008**, *43*, 4356–4362.
25. Ryu, S.; Lee, Y.; Hwang, J.; Hong, S.; Kim, C.; Park, T. G.; Lee, H.; Hong, S. H. High-Strength Carbon Nanotube Fibers Fabricated by Infiltration and Curing of Mussel-Inspired Catecholamine Polymer. *Adv. Mater.* **2011**, *23*, 1971–1975.
26. Naraghi, M.; Filleter, T.; Moravsky, A.; Locascio, M.; Loutfy, R. O.; Espinosa, H. D. A Multiscale Study of High Performance Double-Walled Nanotube–Polymer Fibers. *ACS Nano* **2010**, *4*, 6463–6476.
27. Xu, Z.; Gao, C. Graphene Chiral Liquid Crystals and Macroscopic Assembled Fibres. *Nat. Commun.* **2011**, *2*, 571.
28. Dong, Z.; Jiang, C.; Cheng, H.; Zhao, Y.; Shi, G.; Jiang, L.; Qu, L. Facile Fabrication of Light, Flexible and Multifunctional Graphene Fibers. *Adv. Mater.* **2012**, *24*, 1856–1861.
29. Wei, X.; Naraghi, M.; Espinosa, H. D. Optimal Length Scales Emerging from Shear Load Transfer in Natural Materials: Application to Carbon-Based Nanocomposite Design. *ACS Nano* **2012**, *6*, 2333–2344.
30. Bhattacharyya, A. R.; Sreekumar, T. V.; Liu, T.; Kumar, S.; Ericson, L. M.; Hauge, R. H.; Smalley, R. E. Crystallization and Orientation Studies in Polypropylene/Single Wall Carbon Nanotube Composite. *Polymer* **2003**, *44*, 2373–2377.
31. Ramanathan, T.; Abdala, A. A.; Stankovich, S.; Dikin, D. A.; Herrera-Alonso, M.; Piner, R. D.; Adamson, D. H.; Schniepp, H. C.; Chen, X.; Ruoff, R. S.; *et al.* Functionalized Graphene Sheets for Polymer Nanocomposites. *Nat. Nanotechnol.* **2008**, *3*, 327–331.
32. Rafiee, M. A.; Rafiee, J.; Wang, Z.; Song, H.; Yu, Z.; Koratkar, N. Enhanced Mechanical Properties of Nanocomposites at Low Graphene Content. *ACS Nano* **2009**, *3*, 3884–3890.
33. Andrews, R.; Jacques, D.; Rao, A. M.; Rantell, T.; Derbyshire, F.; Chen, Y.; Chen, J.; Haddon, R. C. Nanotube Composite Carbon Fibers. *Appl. Phys. Lett.* **1999**, *75*, 1329–1331.
34. Chae, H. G.; Minus, M. L.; Rasheed, A.; Kumar, S. Stabilization and Carbonization of Gel Spun Polyacrylonitrile/Single Wall Carbon Nanotube Composite Fibers. *Polymer* **2007**, *48*, 3781–3789.
35. Liu, Y.; Chae, H. G.; Kumar, S. Gel-Spun Carbon Nanotubes/Polyacrylonitrile Composite Fibers. Part III: Effect of Stabilization Conditions on Carbon Fiber Properties. *Carbon* **2011**, *49*, 4487–4496.
36. Dzenis, Y. A. Spinning Continuous Fibers for Nanotechnology. *Science* **2004**, *304*, 1917–1919.
37. Inagaki, M.; Yang, Y.; Kang, F. Carbon Nanofibers Prepared *via* Electrospinning. *Adv. Mater.* **2012**, 2547–2566.
38. Dzenis, Y. A.; Wen, Y. In Continuous Carbon Nanofibers for Nanofiber Composites. MRS Proceedings, MRS Fall Meeting, November 2001.
39. Ko, F.; Gogotsi, Y.; Ali, A.; Naguib, N.; Ye, H.; Yang, G. L.; Li, C.; Willis, P. Electrospinning of Continuous Carbon Nanotube-Filled Nanofiber Yarns. *Adv. Mater.* **2003**, *15*, 1161–1165.
40. Hou, H.; Ge, J. J.; Zeng, J.; Li, Q.; Reneker, D. H.; Greiner, A.; Cheng, S. Z. D. Electrospun Polyacrylonitrile Nanofibers Containing a High Concentration of Well-Aligned Multiwall Carbon Nanotubes. *Chem. Mater.* **2005**, *17*, 967–973.
41. Maitra, T.; Sharma, S.; Srivastava, A.; Cho, Y.; Madou, M.; Sharma, A. Improved Graphitization and Electrical Conductivity of Suspended Carbon Nanofibers Derived from Carbon Nanotube/Polyacrylonitrile Composites by Directed Electrospinning. *Carbon* **2012**, *50*, 1753–1761.
42. Prilutsky, S.; Zussman, E.; Cohen, Y. The Effect of Embedded Carbon Nanotubes on the Morphological Evolution during the Carbonization of Poly(acrylonitrile) Nanofibers. *Nanotechnology* **2008**, *19*, 165603.
43. Prilutsky, S.; Zussman, E.; Cohen, Y. Carbonization of Electrospun Poly(acrylonitrile) Nanofibers Containing Multiwalled Carbon Nanotubes Observed by Transmission Electron Microscope with *in Situ* Heating. *J. Polym. Sci., Part B: Polym. Phys.* **2010**, *48*, 2121–2128.
44. Sreekumar, T. V.; Liu, T.; Min, B. G.; Guo, H.; Kumar, S.; Hauge, R. H.; Smalley, R. E. Polyacrylonitrile Single-Walled

Carbon Nanotube Composite Fibers. *Adv. Mater.* **2004**, *16*, 58–61.
45. Ge, J. J.; Hou, H.; Li, Q.; Graham, M. J.; Greiner, A.; Reneker, D. H.; Harris, F. W.; Cheng, S. Z. D. Assembly of Well-Aligned Multiwalled Carbon Nanotubes in Confined Polyacrylonitrile Environments: Electrospun Composite Nanofiber Sheets. *J. Am. Chem. Soc.* **2004**, *126*, 15754–15761.
46. Guo, H.; Sreekumar, T. V.; Liu, T.; Minus, M.; Kumar, S. Structure and Properties of Polyacrylonitrile/Single Wall Carbon Nanotube Composite Films. *Polymer* **2005**, *46*, 3001–3005.
47. Kim, Y. A.; Muramatsu, H.; Hayashi, T.; Endo, M.; Terrones, M.; Dresselhaus, M. S. Thermal Stability and Structural Changes of Double-Walled Carbon Nanotubes by Heat Treatment. *Chem. Phys. Lett.* **2004**, *398*, 87–92.
48. Bandow, S.; Chen, G.; Sumanasekera, G. U.; Gupta, R.; Yudasaka, M.; Iijima, S.; Eklund, P. C. Diameter-Selective Resonant Raman Scattering in Double-Wall Carbon Nanotubes. *Phys. Rev. B* **2002**, *66*, 075416.
49. Tuinstra, F.; Koenig, J. L. Characterization of Graphite Fiber Surfaces with Raman Spectroscopy. *J. Compos. Mater.* **1970**, *4*, 492–499.
50. Anderson, D. P. *Carbon Fiber Morphology, II: Expanded Wide-Angle X-Ray Diffraction Studies of Carbon Fibers*. Technical Report for the Air Force System Command, Wright-Patterson Air Force Base, OH, February **1991**.
51. Koganemaru, A.; Bin, Y.; Agari, Y.; Matsuo, M. Composites of Polyacrylonitrile and Multiwalled Carbon Nanotubes Prepared by Gelation/Crystallization from Solution. *Adv. Funct. Mater.* **2004**, *14*, 842–850.
52. Li, X. QPCED2.0: a Computer Program for the Processing and Quantification of Polycrystalline Electron Diffraction Patterns. *J. Appl. Crystallogr.* **2012**, *45*, 862–868.
53. Kurban, Z.; Lovell, A.; Jenkins, D.; Bennington, S.; Loader, I.; Schober, A.; Skipper, N. Turbostratic Graphite Nanofibres from Electrospun Solutions of PAN in Dimethylsulphoxide. *Eur. Polym. J.* **2010**, *46*, 1194–1202.
54. Morgan, P. *Carbon Fibers and Their Composites*; CRC Press, Taylor & Francis Group, LLC: Boka Raton, FL, 2005.
55. Arshad, S. N.; Naraghi, M.; Chasiotis, I. Strong Carbon Nanofibers from Electrospun Polyacrylonitrile. *Carbon* **2011**, *49*, 1710–1719.
56. Bhushan, B.; Ling, X.; Jungen, A.; Hierold, C. Adhesion and Friction of a Multiwalled Carbon Nanotube Sliding against Single-Walled Carbon Nanotube. *Phys. Rev. B: Condens. Matter Mater. Phys.* **2008**, *77*, 165428.
57. Frankland, S. J. V.; Caglar, A.; Brenner, D. W.; Griebel, M. Molecular Simulation of the Influence of Chemical Cross-Links on the Shear Strength of Carbon Nanotube-Polymer Interfaces. *J. Phys. Chem. B* **2002**, *106*, 3046–3048.
58. Yu, M.; Yakobson, B. I.; Ruoff, R. S. Controlled Sliding and Pullout of Nested Shells in Individual Multiwalled Carbon Nanotubes. *J. Phys. Chem. B* **2000**, *104*, 8764–8767.
59. Barber, A. H.; Cohen, S. R.; Wagner, H. D. Measurement of Carbon Nanotube–Polymer Interfacial Strength. *Appl. Phys. Lett.* **2003**, *82*, 4140–4142.
60. Andrews, R.; Weisenberger, M. C. Carbon Nanotube Polymer Composites. *Curr. Opin. Solid State Mater. Sci.* **2004**, *8*, 31–37.
61. Saha, B.; Schatz, G. C. Carbonization in Polyacrylonitrile (PAN) Based Carbon Fibers Studied by ReaxFF Molecular Dynamics Simulations. *J. Phys. Chem. B* **2012**, *116*, 4684–4692.
62. van Duin, A. C. T.; Dasgupta, S.; Lorant, F.; Goddard, W. A. ReaxFF: A Reactive Force Field for Hydrocarbons. *J. Phys. Chem. A* **2001**, *105*, 9396–9409.
63. Chenoweth, K.; van Duin, A. C. T.; Goddard, W. A. ReaxFF Reactive Force Field for Molecular Dynamics Simulations of Hydrocarbon Oxidation. *J. Phys. Chem. A* **2008**, *112*, 1040–1053.
64. Kamat, A. M.; van Duin, Adri C. T.; Yakovlev, A. Molecular Dynamics Simulations of Laser-Induced Incandescence of Soot Using an Extended ReaxFF Reactive Force Field. *J. Phys. Chem. A* **2010**, *114*, 12561–12572.
65. Jiang, D.; van Duin, Adri C. T.; Goddard, W. A.; Dai, S. Simulating the Initial Stage of Phenolic Resin Carbonization *via* the ReaxFF Reactive Force Field. *J. Phys. Chem. A* **2009**, *113*, 6891–6894.
66. Desai, T. G.; Lawson, J. W.; Keblinski, P. Modeling Initial Stage of Phenolic Pyrolysis: Graphitic Precursor Formation and Interfacial Effects. *Polymer* **2011**, *52*, 577–585.
67. Morita, K.; Murata, Y.; Ishitani, A.; Murayama, K.; Ono, T.; Nakajima, A. Characterization of Commercially Available PAN (Polyacrylonitrile)-Based Carbon Fibers. *Pure Appl. Chem.* **1986**, *58*, 455–468.
68. Ko, T. H. The Influence of Pyrolysis on Physical Properties and Microstructure of Modified PAN Fibers during Carbonization. *J. Appl. Polym. Sci.* **1991**, *43*, 589–600.
69. Liu, J.; Wang, P. H.; Li, R. Y. Continuous Carbonization of Polyacrylonitrile-Based Oxidized Fibers: Aspects on Mechanical Properties and Morphological Structure. *J. Appl. Polym. Sci.* **1994**, *52*, 945–950.